23G11

Gas-Phase Diagnostics and Global Model Simulation of BCl_3-Containing Plasmas

BCl_3混合プラズマの気相診断とモデリング

Shota Sato, Keisuke Nakamura, Yoshinori Takao, Koji Eriguchi and Kouichi Ono
佐藤聖太, 仲村恵右, 鷹尾祥典, 江利口浩二, 斧　高一

Department of Aeronautics and Astronautics, Graduate School of Engineering, Kyoto University
Yoshida-Honmachi, Sakyo-ku, Kyoto 606-8501, Japan
京都大学大学院工学研究科航空宇宙工学専攻, 〒606-8501　京都市左京区吉田本町

Etching characteristics of HfO_2 have been investigated for BCl_3 plasmas. The chemical compositions of BCl_3 plasmas are required to be clarified, to understand the etching mechanisms concerned. We carried out plasma diagnostics using optical emission spectroscopy (OES), quadrupole mass spectrometry (QMS), and Langmuir probe measurements, and calculated the electron temperature and the particle densities by global model simulations. The numerical results were consistent with the experiments to give us rough estimates of BCl_3 plasma compositions. The relationship between the etching mechanisms and plasma compositions is discussed.

1. Introduction

As ULSI device dimensions continue to be scaled down to tens of nanometers, efforts have been made to replace gate silicon oxides and oxynitrides with high-dielectric-constant (k > 20) materials such as HfO_2, ZrO_2, and their silicates and aluminates [1]. However, high-k dielectrics or metal oxides are usually difficult materials to etch, owing to strong metal-oxygen bonds and less volatile metal-halogen compounds; thus, the etch selectivity for high-k/Si is not so high as to be employed in place of wet etching, also owing to highly volatile halogen compounds of Si. High-k dielectrics such as HfO_2 are often etched by BCl_3-containing plasmas [2−7], because BCl_x species tend to form a relatively volatile product, $HfCl_4$, by breaking Hf−O bonds. Previously, we demonstrated highly selective etching of HfO_2 over Si in electron cyclotron resonance (ECR) BCl_3-containing plasmas without rf biasing [5−7]. For further understanding the etching mechanisms, the chemical compositions are required to be clarified in BCl_3 plasmas. This paper presents gas-phase diagnostics and global model simulations of BCl_3-containing plasmas.

2. Experiment and Numerical Model

Etching was performed in ECR and ICP plasma reactors, as shown in Fig. 1. The ECR was a divergent magnetic field type [5−7]; the specimen chamber was 36 cm in diameter and 40 cm in height, containing a 6-in.-diameter electrode (wafer stage) approximately 20 cm downstream from the ECR resonance region. The discharge was established by 2.45-GHz microwave powers of 600 W. The ICP was a planar coil type [8]; the specimen chamber was 25 cm in diameter and 30 cm in height, containing a 4-in.-diameter electrode (wafer stage). The discharge was established by 13.56-MHz rf powers of 400 W. The wafer stage in both ECR and ICP was capacitively coupled to a 13.56-MHz rf power supply for additional rf biasing (P_{rf} < 50 W), where the wafer surface temperature was maintained in the range 70−80°C. In experiments with no bias (P_{rf} = 0 W), the wafer stage was under floating conditions, and no breakthrough step was employed with additional biasing. Feedstock gases were BCl_3, Cl_2, O_2, and Ar at total gas pressures of P_0 = 1−20 mTorr with a total mass flow rate of 40 sccm. Several diagnostics were employed to characterize the plasma around the wafer position: optical emission spectroscopy (OES), quadrupole mass spectrometry (QMS), and Langmuir probe measurements.

Moreover, we employed a well-mixed (zero-dimensional) reactor model, or global model, to investigate the BCl_3 plasma chemistry. In the model, the electron temperature and the particle densities were spatially averaged, and we took into account 14 species (BCl_3, BCl_2, BCl, B, Cl_2, Cl, BCl_3^+, BCl_2^+, BCl^+, Cl_2^+, Cl^+, Cl^-, Cl^*, e) and 36 reaction

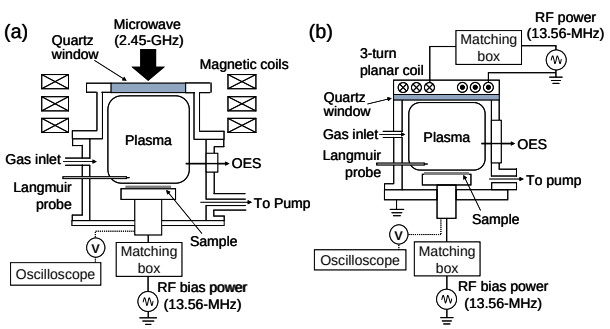

Fig. 1. Schematic diagrams of (a) ECR and (b) ICP plasma reactors used in this study.

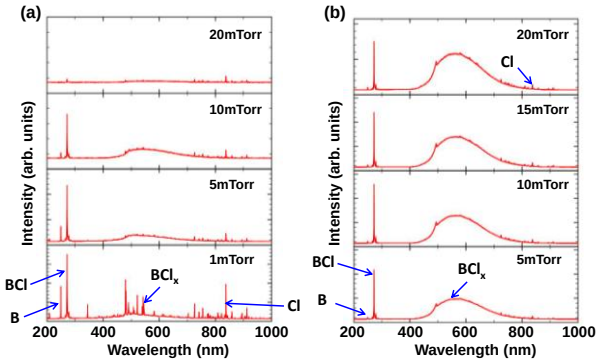

Fig. 2. OES intensities in (a) ECR and (b) ICP BCl_3 plasmas at P_0 = 1−20 mTorr.

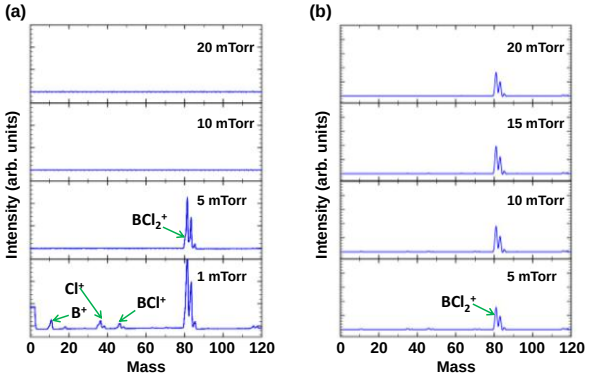

Fig. 3. QMS intensities in (a) ECR and (b) ICP BCl_3 plasmas with the ionizer off at P_0 = 1−20 mTorr.

processes. We calculated the electron temperature and 13 species densities by solving 14 differential equations (13 species continuity equations and a conservation equation of the electron energy), where the electron density was calculated by using the quasi-neutral law. The model assumed that the ion and neutral temperatures were 300 K and the electron velocity distribution was Maxwellian.

3. Results and Discussion

Figure 2 shows the OES intensities of ECR and ICP BCl_3 plasmas at P_0 = 1−20 mTorr. In ECR plasmas, B, BCl, and Cl were detected at lower P_0, while in ICP plasmas, B and Cl were not detected. It is possible that at lower P_0, the electron density was higher in ECR plasmas, causing B and Cl to be formed through electron-impact dissociation of BCl_3 therein.

Figure 3 shows the QMS intensities of ECR and ICP BCl_3 plasmas with the ionizer off at P_0 = 1−20 mTorr. It is noted that BCl_2^+ was the dominating ion species in both ECR and ICP plasmas, and that B^+ and BCl^+ ions were also detected at lower P_0 in ECR plasmas.

Figure 4 shows the Langmuir probe measurements in ECR and ICP BCl_3 plasmas at P_0 = 1−20 mTorr. The ion and electron densities at lower P_0 were higher in ECR than in ICP plasmas, while the densities at high P_0 were lower in ECR than in ICP.

Figure 5 shows the electron temperature and particle densities in BCl_3 plasmas calculated by the global model simulation. Figure 5(a) shows that BCl_2^+ was the dominating ion, which is consistent with the QMS measurements in Fig. 3. On the other hand, Fig. 5(b) shows that Cl is the most abundant neutral radical species, followed by BCl and BCl_2. In the calculation, the densities of all species increased with increasing pressure, while only the Cl^+ density decreased with pressure. This may be explained by the effect of surface recombination of Cl atoms on the chamber walls.

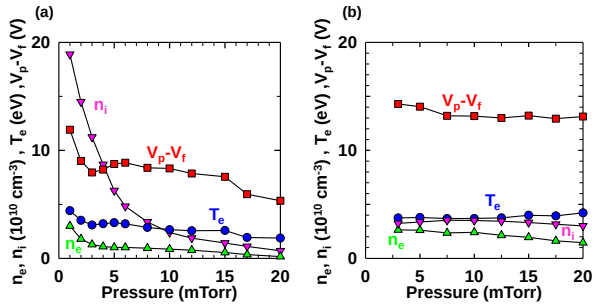

Fig. 4. Langmuir probe measurements in (a) ECR and (b) ICP BCl_3 plasmas at P_0 = 1−20 mTorr.

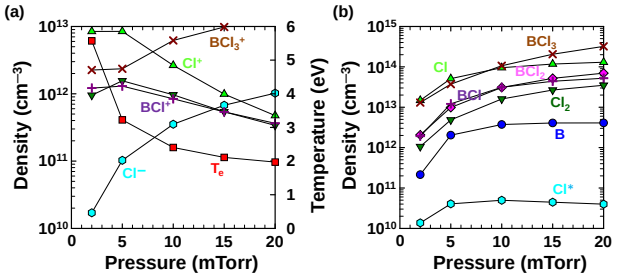

Fig. 5. (a) Electron temperature and densities of charged species, and (b) densities of neutral species in BCl_3 plasmas calculated by the global model simulation (input power: 600 W, mass flow rate: 40 sccm).

References

[1] G. D. Wilk, R. M. Wallace, and J. M. Anthony, J. Appl. Phys. **89**, 5243 (2001).

[2] E. Sungauer *et al.*, J. Vac. Sci. Technol. B **25**, 1640 (2007).

[3] R. Wise *et al.*, Solid State Technol. **Dec**. 18 (2008).

[4] D. Shamiryan *et al.*, Chem. Eng. Comm. **196**, 1475 (2009), and references therein.

[5] K. Nakamura *et al.*, Vacuum **80**, 761 (2006).

[6] T. Kitagawa *et al.*, Jpn. J. Appl. Phys. **45**, L297 (2006).

[7] K. Nakamura *et al.*, Appl. Phys. Express **2**, 016503 (2009).

[8] K. Takahashi *et al.*, J. Vac. Sci. Technol. A **23**, 1691 (2005); **24**, 437 (2006).

[9] E. Meeks *et al.*, J. Vac. Sci. Technol. A **16,** 2227 (1998).